e-ISSN 3050-8460
Journal of Dermatology Research

ATHENAEUM SCIENTIFIC PUBLISHERS

Research Article

Therapeutic Potential of Low-Dose *Trypanosoma Cruzi* Calreticulin in Enhancing Diabetic Wound Healing and Adipose Derived Stem Cells Fibroblastic Behavior

Jose Ignacio Arias[1*], Javiera Parra[1], Alejandra Guerrero-Moncayo[2]

[1]Regenerative Medicine Lab (BiMre), Faculty of Veterinary and Animal Sciences, University of Chile, Santiago

[2]ACCDiS, Faculty of Chemical and Pharmaceutical Sciences, University of Chile, Santiago

***Correspondence author:** Jose Ignacio Arias, Regenerative Medicine Lab (BiMre), Faculty of Veterinary and Animal Sciences, University of Chile, Santiago; Email: iarias@uchile.cl

Citation: Arias JI, et al. Therapeutic Potential of Low-Dose *Trypanosoma Cruzi* Calreticulin in Enhancing Diabetic Wound Healing and Adipose Derived Stem Cells Fibroblastic Behavior. J Dermatol Res. 2025;6(2):1-17.

https://doi.org/10.46889/JDR.2025.6221

Received Date: 31-07-2025

Accepted Date: 17-08-2025

Published Date: 24-08-2025

Abstract

Calreticulin (CRT) is a vital chaperone protein that regulates cellular functions via calcium homeostasis. CRT exhibits diverse roles from intracellular to extracellular functions and can impact immune response, wound healing and more. *Trypanosoma cruzi* Calreticulin (TcCRT) has demonstrated superior wound-healing effects, which merits exploration of its effects in diabetic wound healing. Streptozotocin-induced diabetic rats were used to prepare Adipose-Derived Stem Cells (ADSCs) and to treat dorsal skin wounds. *In-vitro*, isolated rat ADSCs were characterized and induced to differentiate into osteoblasts, adipocytes and fibroblasts. *In-vivo*, diabetic rat wounds were treated with TcCRT at 2.5 ng/µL and 1,000 ng/µL and assessed histologically. Statistical analyses were conducted to assess the results. ADSCs cultured medium with added TcCRT exhibits fibroblastic behavior, expressing high levels of Tenascin-C (TN-C) and Matrix Metalloproteinase-1 (MMP-1) *in-vitro*. *In-vivo*, low-dose TcCRT accelerates re-epithelialization, granulation tissue formation and dermal maturation in diabetic rat wounds. We showed that low TcCRT concentrations are more effective than high doses, suggesting potential therapeutic use for chronic wounds.

Keywords: Calreticulin; Diabetic Rats; Adipose-Derived Stem Cells (ADSCs); Fibroblasts' Skin Wound Healing; Chagas; *Trypanosoma cruzi*

Abbreviations

CRT: Calreticulin; TcCRT: *Trypanosoma cruzi* CRT; HuCRT: Human CRT; ADSCs: Adipose-Derived Stem Cells; TN-C: Tenascin-C;mmP-1: Matrix Metalloproteinase-1; ER: Endoplasmic Reticulum; HBSS: Hank's Balanced Salt Solution; DMEM-HG: High-Glucose Dulbecco's Modified Eagle's Medium; PBS: Phosphate-Buffered Saline; SVF: Stromal Vascular Fraction; ON: Osteonectin; PPARγ2: Proliferator-Activated Receptor-γ; RT-PCR: Reverse Transcription Polymerase Chain Reaction; CTGF: Human Connective Tissue Growth Factor; ANOVA: Factorial Analysis of Variance

Introduction

Calreticulin (CRT) is a chaperone calcium-binding protein of the Endoplasmic Reticulum (ER) that works by directing the proper folding of proteins and by controlling many cellular functions through homeostatic control of calcium levels of the cytosol and the ER [1]. CRT is widely distributed in animal, plant and protozoa eukaryotic cells and in mammals' CRT has been considered a stress-related protein [2-4].

Currently, it is known that mammalian CRT and other classic intracellular chaperone proteins are emerging as molecules that also direct biological activities from the cell surface and extracellular space, thereby acting as important dual mediators of physiological and pathological processes including immune response, angiogenesis, phagocytosis, fibrosis and tissue healing processes [1,5]. A detailed description of such functions has been recently reviewed [6]. CRT's extracellular functions have been

analyzed in several *in-vitro* and *in-vivo* studies, where it has been demonstrated that CRT plays an important role in the healing of cutaneous wounds and various processes associated with cutaneous repair, such as modulation of angiogenesis, promotion of cell adhesion and also in antitumor effects [2,3,5]. CRT expression is up-regulated by factors that are recognized to induce both ER stress and fibrosis, including hyperglycemia, oxidative stress, cigarette smoke, hypoxia and a TGF-β-rich environment [6-11].

Similarly, in pigs' experimental models, topical administration of CRT has been shown to significantly improve wound healing pace and quality [12]. Additionally, treatment with human and rabbit CRT increases the rate of re-epithelialization, promotes the migration and proliferation of keratinocytes and fibroblasts and increases the amount of granulation tissue in a genetically (db/db) leptin receptor-deficient mouse strain, resulting in a significant reduction in the time to complete wound closure when compared to untreated wounds [13]. Furthermore, CRT has been found *in-vivo* to be more effective than PDGF-BB, the only FDA-approved recombinant protein for chronic wounds, in encouraging wound healing [12]. According to these investigations, CRT has encouraging potential as a topical therapeutic agent for the treatment of chronic wounds, including those in diabetes patients [1].

CRT has also been found in *Trypanosoma cruzi*, a flagellated protozoan parasite responsible for Chagas disease [14]. Unlike other trypanosomes, *T. cruzi* cycles between extracellular and intracellular stages, generating different interactions with the host. One of the molecules involved in the host-parasite interaction is *T. cruzi* Calreticulin (TcCRT). This protein has been found in the ER, on the surface of the parasite membrane and outside the parasite [2,15]. TcCRT is 50% homologous to Human CRT (HuCRT) and they share several functions [16]. However, TcCRT is three times more efficient in molar terms than HuCRT, greatly increasing the proliferation and migration of human fibroblasts *in-vitro* and has a greater antiang iogenic and antitumor effect [2,16]. These differential effects observed *in-vitro* correlate with those obtained *in-vivo*. When applied to experimental skin wounds, TcCRT is more effective than HuCRT in accelerating wound healing [2].

While the effect of externally added TcCRT on normal rat skin wound healing has been reported, there are no reports on the use of this parasite protein in the wound-healing process of diabetic rats, either *in-vitro* or *in-vivo* [3]. In the study described herein, we investigated the effects of TcCRT on both *in-vitro* differentiation of diabetic rat ADSCs and *in-vivo* wound healing of diabetic rat skin.

Materials and Methods

All animal procedures were approved by the local Animal Bioethics Committee and all animals received humane care in accordance with the Guide for the Care and Use of Laboratory Animals prepared by the National Academy of Sciences and published by the National Institutes of Health (NIH publication No. 85-23, revised 1985).

Diabetic Rat Model

Diabetes mellitus was induced in 12 adult male Sprague-Dawley rats weighing 400-450 g, based on the standardized model of experimental diabetes described by Velez, et al., with a sing le intraperitoneal injection of streptozotocin at a dose of 55 mg/kg. The streptozotocin was dissolved in 1X Hank's Balanced Salt Solution (HBSS) (HyCloneTM) and sterilized with Minisart® PES 0.2 μm syring e filters. After 48 hours the rats were subjected to blood glucose tests with a glucose meter (Accu-Chek® Advantage). Those with sustained blood glucose levels greater than 200 mg/dL at 48 hours and six days were considered diabetic and were used for experimental procedures [17]. The animals were housed in individual cages in a controlled environment at a temperature of 24°C and a constant humidity of 45%. The animals were fed commercial pellets and water ad libitum throughout the duration of the experiment. Weight, food and water consumption were monitored throughout the experimental periods. After the sixth day, rats underwent surgery. Inhalation anesthesia with 2% isoflurane was used for all 12 rats, inside an anesthetic chamber for induction and a face mask for maintenance. Three rats were used for ADSCs collection and 9 for performing the skin wounds *in-vivo* experiments.

In-vitro Experiments

Fat Collection and ADSC Isolation

In three of the diabetic rats, both ing uinal and ventral subcutaneous fat was collected through a sterile surgical procedure. Then the rats were euthanized by intracardiac injection of 5% sodium thiopental. The fat tissue was washed four times with an equal

volume of Phosphate-Buffered Saline (PBS) containing antibiotics (100 U/mL penicillin, 100μg/mL streptomycin and 0.25μg/mL amphotericin B) (HyClone®, South Logan, Utah, USA) to remove contaminant cells. The sample was then incubated in 1 mL of 0.5% collagenase (Sigma Aldrich®, St. Louis, Missouri, USA) per gram of fat and agitated at 37°C for 45 min. The enzymatic reaction was inactivated with an equal volume of High-glucose Dulbecco's Modified Eagle's medium (DMEM-HG; HyClone®, South Logan, Utah, USA). The solution was filtered through a tissue culture 100μm cell strainer to remove undigested tissue and centrifuged at 770 x G for 7 minutes [18].

The supernatant was discarded and a Stromal Vascular Fraction (SVF) pellet was collected. The SVF consists of a heterogeneous cell population including circulating blood cells, fibroblasts, pericytes and endothelial cells as well as "preadipocytes" or adipocyte progenitor cells. Thus, the floating population of mature adipocytes in the supernatant was discarded and the SVF pellet was retained, washed with DMEM-HG and filtered through a 60-μm cell strainer.

The final SVF cell fraction was counted in a Neubauer chamber and seeded into 75cm² cell culture flasks (Orang e Scientific®, Braine-l'Alleud, Belgium) at 1,000-3,500 cells/cm² in DMEM-HG, 10% FBS, 1% antibiotic/antimycotic (10 U/mL penicillin, 10 mg/mL streptomycin and 25μg/mL amphotericin B) (all from HyClone, South Logan, Utah, USA) [18]. Cultures were washed after 72 h to remove unattached cells and expansion medium was changed every 48 h thereafter. To keep cells at low density, which minimizes cell death and spontaneous differentiation, the cultures were passaged when the cells reached 80% of confluence. The plastic-adherent cells were harvested with trypsin-EDTA 0.25% (HyClone®, South Logan, Utah, USA) for 3 min at 37°C, followed by trypsin inactivation with 2 volumes of culture medium containing serum. The cells were counted and plated into 25cm² culture flasks at a density of 5,000 cells/cm². Cultures were passaged three times after the cells achieved a density of 70-80% and the cells were stored at -80°C in cryopreservation medium (10% dimethylsulfoxide, 60% DMEM-HG, 30% FBS) at 6 x 105 cells/cryovial after the third passage [18].

Flow Cytometry Analysis

Flow cytometry analysis was performed using 5 × 105 third to fourth passage ADSCs (in 100μL of PBS) incubated with different fluorescent-labeled monoclonal antibodies (anti-rat CD45-PE-Cy5, anti-rat CD73-FITC, anti-rat CD105-FITC and anti-rat CD90-FITC; Biolegend, Cheng du, Sichuan, P.R. China). For antibody labeling, cells were incubated in the dark at 2-8°C for 30 minutes. After washing twice with PBS, cells were resuspended in 300μL of PBS and analyzed with a FACScalibur flow cytometer (Becton Dickinson, Mountain View, CA).

Osteogenic and Adipogenic Differentiation

Third passage ADSCs were seeded into 25-cm² cell culture flasks (2 x 10^4 cells per flask). Control culture medium consisted of α-MEM (HyClone®, South Logan, Utah, USA) supplemented with 10% FBS and 1% antibiotic/antimycotic (10 U/mL penicillin, 10 mg/mL streptomycin and 25μg/mL amphotericin B) (HyClone®, South Logan, Utah, USA). The differentiation medium for osteogenesis consisted of the control culture medium supplemented with 1μM dexamethasone, 10mm β-glycerophosphate, 2mm L-glutamine and 50μM ascorbic acid (all from Sigma Aldrich®, St. Louis, Missouri, USA.). Concurrently, adipogenesis was stimulated with differentiation medium consisting of control medium containing 1μM dexamethasone, 0.5 mm indomethacin (Sigma Aldrich®, St. Louis, Missouri, USA), 10 μg/mL insulin (Gibco®, Grand Island, New York, USA and 100 mm 3-isobutyl-1-methylxanthine (Sigma Aldrich®, St. Louis, Missouri, USA). Cells were cultured in differentiation medium for three days and then in differentiation maintenance medium containing DMEM-HG, 10% FBS, 1% antibiotic/antimycotic supplemented with 10 μg/mL insulin [18]. Experimental and control culture mediums were chang ed every three days.

Cells were obtained at day 28 and analyzed for Osteonectin (ON) expression as a measure of osteogenic differentiation and for Peroxisome Proliferator-Activated Receptor-γ (PPARγ2) expression as a measure of adipogenic differentiation. Expression analysis was done by Reverse Transcription Polymerase Chain Reaction (RT-PCR). β-ACTIN gene expression was used as a housekeeping control. The level of osteogenic differentiation was also analyzed at day 21 by visualization of mineralized matrix in the cell culture by von Kossa stain and adipogenic visualization by staining intracellular accumulation of lipid vacuoles with Oil Red O. As positive controls rat osteoblasts and adipocytes were used, respectively.

Fibroblast Differentiation

The isolated cells from rat adipose tissue were seeded in either control or differentiation medium into 25cm^2 cell culture flasks (2 x 10^4 cells per flask). Control medium consisted of DMEM-HG supplemented with 10% FBS and 1% antibiotic/antimycotic. Differentiation medium consisted of control medium supplemented with 50 *ng/mL* human Connective Tissue Growth Factor (CTGF) (Sigma Aldrich®, St. Louis, Missouri, USA) [19]. Experimental and control culture mediums were chang ed every three days.

Samples were obtained at day 28 and analyzed for TN-C andmmP-1 expression by RT-PCR. The level of fibroblast differentiation was also analyzed at day 21 by visualization of collagen fibers stainable with Mallory's trichrome stain. As positive control, rat skin fibroblasts were used.

TcCRT-Supplemented Cell Culture

ADSCs were seeded with either control or supplemented medium into 25-cm^2 cell culture flasks (2 x 10^4 cells per flask). Control medium consisted of DMEM-HG supplemented with 10% FBS and 1% antibiotic/antimycotic. Supplemented medium consisted of control medium containing 0.01μg/mL TcCRT as described elsewhere [2]. Both supplemented and control mediums were changed every three days. The level of differentiation to a fibroblastic lineage was analyzed as described above for fibroblast differentiation. As positive control, rat skin fibroblasts were used.

RNA Extraction and cDNA Synthesis

Total RNA from cell cultures was extracted with the Qiagen RNeasy kit (Qiagen, Hilden, Germany) following the manufacturer's recommendations. Total RNA concentration and purity of each sample were determined with an Epoch Microplate spectrophotometer (BioTek, Winooski, Vermont, USA). After quantification, RNA was treated with DNase I (RNase-free) (New Eng land Biolabs, Ipswich, Massachusetts, USA) to eliminate contaminating genomic DNA. The complementary DNA (cDNA) synthesis was obtained by Reverse Transcription reaction (RT) with Reverse Transcription System (Promega, Madison, Wisconsin, USA) according to the manufacturer's protocol.

RT-PCR

PCR rat primers were created with FastPCR v6.6 software and fabricated by IDT (Coralville, Iowa, USA).

Each PCR reaction (20μL) was performed with 2.5μL of 10x Paq5000 Reaction Buffer, 0.2μL of 100mm dNTP mix (25mm each dNTP), 1.25 U of Paq5000 Polymerase DNA (all from Qiagen, Hilden, Germany) (5 U/μL), 0.5μL of 10μM forward primer (IDT), 0.5μL of 10μM reverse primer (IDT), 1μL of cDNA as template and nuclease-free water (Qiagen) to a final volume of 20μL. The PCR amplification reaction was carried out in a PCR Express Thermal Cycler (Thermo Hybaid, Ashford, Kent, Eng land). The PCR reaction conditions consisted of an initial denaturation at 95°C for 2 minutes, followed by 30 cycles of denaturation at 95°C for 20 seconds, an annealing cycle at the corresponding temperature for each primer for 20 seconds, an extension cycle at 72°C for 30 seconds, a final extension at 72°C for 5 minutes and cooling at 4°C. The amplified cDNA fragments were run through 2% horizontal agarose gel electrophoresis and the gel was stained with 0.05μL/mL GelRed Nucleic Acid Gel Stain, 10,000x in DMSO (Biotium, Hayward, California, USA). PCR products were visualized and digitized with an ultraviolet transilluminator (Wealtec, Sparks, Nevada, USA). mRNA expression levels were normalized with the housekeeping β-actin content in the mRNA samples. Image pixels were then quantified with National Institutes of Health ImageJ v1.37 software (NIH ImageJ), measuring with the tool Analyze Gel Plot lanes.

In-vivo experiments

Full Thickness Dorsal Skin Wounds

Nine diabetic rats were divided into three groups. Three total thickness wounds of the retroscapular dorsal skin were created in the nine rats with a 6 mm diameter Kruuse® excisional biopsy punch under general inhalation anesthesia. To avoid contraction of the wound produced by the panniculus muscle that is located immediately below the dermis, 0.5 mm thick circular polypropylene splinters with an internal diameter of 6 mm (size of the wound) were fixed around the wound edges, exposing the wound in its center, which provided a more suitable model to simulate human skin wound healing [20].

TcCRT Preparation and Treatments

TcCRT was cloned, amplified and expressed as previously described (Ferreira et al., 2004b). Briefly, DNA coding for TcCRT was isolated from a genomic library in the Xgt11 phage. TcCRT, without its leader and KEDL ER retention sequence, was amplified by PCR and ligated into the pET-28b+ vector (Novagen, Darmstadt, Germany) in EcoRI restriction sites.

A topical dose of 10μL of TcCRT was applied every other day in 2 of the 3 wounds. In the first wound a high concentration of 1μg/μL, in the second, a low concentration of 2.5 ng/μL and the third wound acted as a negative control with only HBSS (Fig. 1).

Wound Perimeter

Digital photographs were taken of the wounds of all rats at surgical day 0. Then digital photographs were taken of the three rats of each group at 5, 10 and 30 days of healing (5, 10 and 30). Wound healing was analyzed with National Institutes of Health ImageJ v1.37 software (NIH ImageJ) by measuring the perimeter of the contracting wound and expressing this as the percentage of the original wound at time 0.

Histological Analysis

Wounds were left open (rather than being stitched together) and left to heal by itself, filling in and closing up naturally for 0, 5, 10 and 30 days. At the end of each time period, the three rats of each group were euthanized in a CO_2-saturated chamber. The wounds were immediately removed along with the adjacent margin of normal skin. The tissue was fixed in Glyo-Fixx™. Then the samples were embedded and cross-sectioned at 0.5μm thickness and the tissue sections were mounted on glass slides and stained with hematoxylin-eosin. Finally, four tissue sections were selected for each experimental wound for further histological double-blind analysis, which was carried out by two independent trained researchers unaware of the treatment received by each wound. The digitization of the tissue sections was done with a Motic AE31 microscope fitted with a Moticam Pro 282A camera and Motic Images Plus v 2.0 scanning software.

Re-Epithelialization

Re-epithelialization measurements were done by measuring the distance between the advancing edges of keratinocyte migration over the wound bed and were expressed as the percentage of the total wound length measurements as described elsewhere [3].

Granulation Tissue Formation/Neodermal Depth Assessment

Neodermal depth measurements were performed for the wound area from the dermal-epidermal junction down to the underlying discontinuous panniculus muscle. The results were expressed as a percentage of the height of normal rat dermis (1.5 ± 0.062 mm).

Neodermis Cell Count/Neodermis Maturity Assessment

The cells present in neodermis between the collagen fibers were manually counted. Density was expressed as number of cells/mm^2. Data were compared with the average number of cells of normal rat dermis (9.6 cells/nm^2).

Statistical Analysis

For the *in-vitro* ADSC experiments, gene relative expression RT-PCR was performed in quadruplicate and the results were expressed as mean ± SD for n = 4. Statistical analysis was performed on the four treatments and the negative control by factorial Analysis of Variance (ANOVA). Statistical analyses for all experiments were performed with the SPSS v12 software (Chicago, IL, USA) and Infostat software (Córdoba, Argentina).

For *in-vivo* skin wound healing experiments, statistical analysis on the wound treatments and the negative control was performed by ANOVA. Statistical analyses for all experiments were performed with the SPSS v12 software (Chicago, IL, USA) and Infostat software (Córdoba, Argentina).

Results

Rat ADSC Characterization

Within three to four passages after initial plating of the primary culture, rat ADSCs showed a spindle-shaped fibroblastic morphology. Confluent rat ADSCs appeared to be a mono-layer of large, flat cells. Flow cytometry analysis of these rat ADSCs showed positive reaction to the cell surface proteins CD105, CD73 and CD90 and negative reaction for CD45 (Fig. 2). Rat ADSCs did not spontaneously differentiate during culture expansion.

When cultured in lineage-specific differentiation culture medium, rat ADSCs underwent osteogenic (Fig. 3,4) and adipogenic (Fig. 5) differentiation. In fact, when cultured in osteogenic differentiation culture medium, positive von Kossa stain indicating the formation of mineralized bone matrix (Fig. 4) and RT-PCR for ON gene expression were significantly higher in the differentiated ADSCs than the positive and negative control cells (Fig. 4). When cultured in adipogenic differentiation culture medium, positive Oil Red O stain, indicative of the formation of adipocytic lipid vacuoles, occurred in a limited number of ADSCs (Fig. 5) and RT-PCR gene expression for PPAR-γ2 mRNA was not detectable (Fig. 5).

In CTGF fibroblastic differentiation culture medium, rat ADSCs showed abundant spindle-shaped cells surrounded by Mallory's trichrome blue-stained fibrillar bundles indicative of collagen fibers (Fig. 6) and a higher RT-PCR TN-C gene expression than the negative control cells (Fig. 6).

Rat ADSC Differentiation in Added TcCRT Medium

By four weeks of culture in Added TcCRT medium, cells showed a spindle-shaped fibroblastic morphology, indisting uishable from that of ADSCs cultured in non-conditioned medium (Fig. 7). In contrast, bundles of collagen that are stained positive by the Mallory trichrome stain were abundant in the Added TcCRT ADSC cultures (Fig. 7) and were not appreciable in control ADSC cultures (Fig. 7). In addition, mRNA expression of the specific fibroblastic differentiation markers TN-C andmmP-1 was significantly higher for the Added TcCRT medium ADSC cells than the negative control cells, with no significant differences from the expression by the CTGF-induced fibroblast cells used as a positive control.

Macroscopic Wound Healing Perimeter Chang es

Wound perimeter chang es over time in response to different treatments are shown in Fig. 8. The best results were obtained with the low concentration of TcCRT (2.5ng /μL). Between the day of injury and day five of healing there were no significant differences between the treatments and the control wounds ($p>0.05$). However, at ten days and 30 days the greatest effect on wound healing at the macroscopic level was observed with the low concentration of TcCRT (2.5ng /μL) ($p<0.05$), where there was a greater decrease in the perimeter of the wounds, reaching a perimeter of only 3.4 ± 0.6 mm compared to the initial 17 mm. The changes in wound perimeter can also be seen in Fig. 9, where it is macroscopically evident that at day 10 the wound treated with the low dose of TcCRT has a smaller blood clot remaining and less skin irritation.

Re-Epithelialization

All of the treatments at the different times of wound healing had significant differences between them ($p<0.05$). The maximum effect of re-epithelialization was obtained with 2.5 *ng/μL* TcCRT, achieving 100% re-epithelialization at 30 days of treatment (Fig. 10), while wounds that did not receive TcCRT treatment showed the lowest percentages of re-epithelialization at each time of measurement. After five days of healing, a low percentage of re-epithelialization of 4.9% was observed in the control wounds. This percentage was three times less compared to the high and low doses of TcCRT. After ten days the wounds treated with the low concentration of TcCRT reached a percentage of wound closure of 53.6%, while the untreated wounds and those treated with the high concentration of TcCRT had a re-epithelialization percentage of 14.3% and 32.3%, respectively. At 30 days, only the wounds treated with the low concentration of TcCRT reached complete closure of the wound (100% re-epithelialization).

Granulation Tissue Depth

It was observed that the greatest effect on granulation tissue formation was obtained with 2.5 ng/μL TcCRT, while the granulation tissue results for the negative control and the treatment with 1,000 g/μL TcCRT were not significantly different ($p>0.05$) and show less granulation tissue depth formation (Fig. 11). After five days of healing, the untreated wounds and those treated with 1,000 ng/μL TcCRT reached only 14% of the normal depth of the neodermis (0.21-0.22 mm). On the other hand, the wounds treated with 2.5 ng/μL TcCRT reached a height of the neodermis twice that of the other two treatments, that is, 27% of the depth of

normal rat dermis. After ten days of healing, the wounds treated with 2.5 ng/μL TcCRT reached 71% of the normal depth of the neodermis (1.07 mm), whereas the control wounds and the wounds treated with 1,000 ng/μL TcCRT showed less formation of granulation tissue, reaching 31% (0.47 mm) and 26% (0.39 mm), respectively. At 30 days of healing, the neodermis of the wounds treated with 2.5 ng/μL TcCRT managed to reach 90% of normal (1.35mm), while the control wounds and the wounds treated with 1,000 ng/μL TcCRT did not show significant differences and reached only 63% of the normal neodermis depth (0.95 mm).

Cell Density

To evaluate the maturation rate of the dermis, cell density was determined and cell count was expressed in cells/mm^2. Fig. 12 shows the cell density of the dermis of the wounds for each of the treatments at five, ten and 30 days of healing . The percentage was determined compared to the average number of dermal cells in a normal rate (approximatel 9.6 cells/mm^2). After five and ten days of healing, wounds treated with 2.5 ng/μL TcCRT showed a significantly higher cellularity than wounds treated with 1,000 ng/μL TcCRT and the HBSS control wounds ($p<0.05$). However, on day 30 of healing, wounds treated with 2.5 *ng/μL* TcCRT had a significant decrease in cellularity that almost reached the normal dermal cellularity level.

Thus, the overall trends in cell density show differences for the different treatments. After five days of healing, the wounds that received the low concentration of TcCRT presented a cellularity twice as high as that of normal dermis, while the control wounds and the wounds treated with the high concentration of TcCRT had no significant differences from normal rat dermis. At ten days of healing, wounds treated with the low TcCRT concentration had a cell density three times higher than that of normal dermis, while untreated wounds and wounds treated with a high TcCRT concentration exhibited cellularity twice as high as normal dermis. After 30 days of healing, treatment with the low TcCRT concentration was more effective, reaching a greater maturity of the dermis compared to treatment with the high concentration of TcCRT.

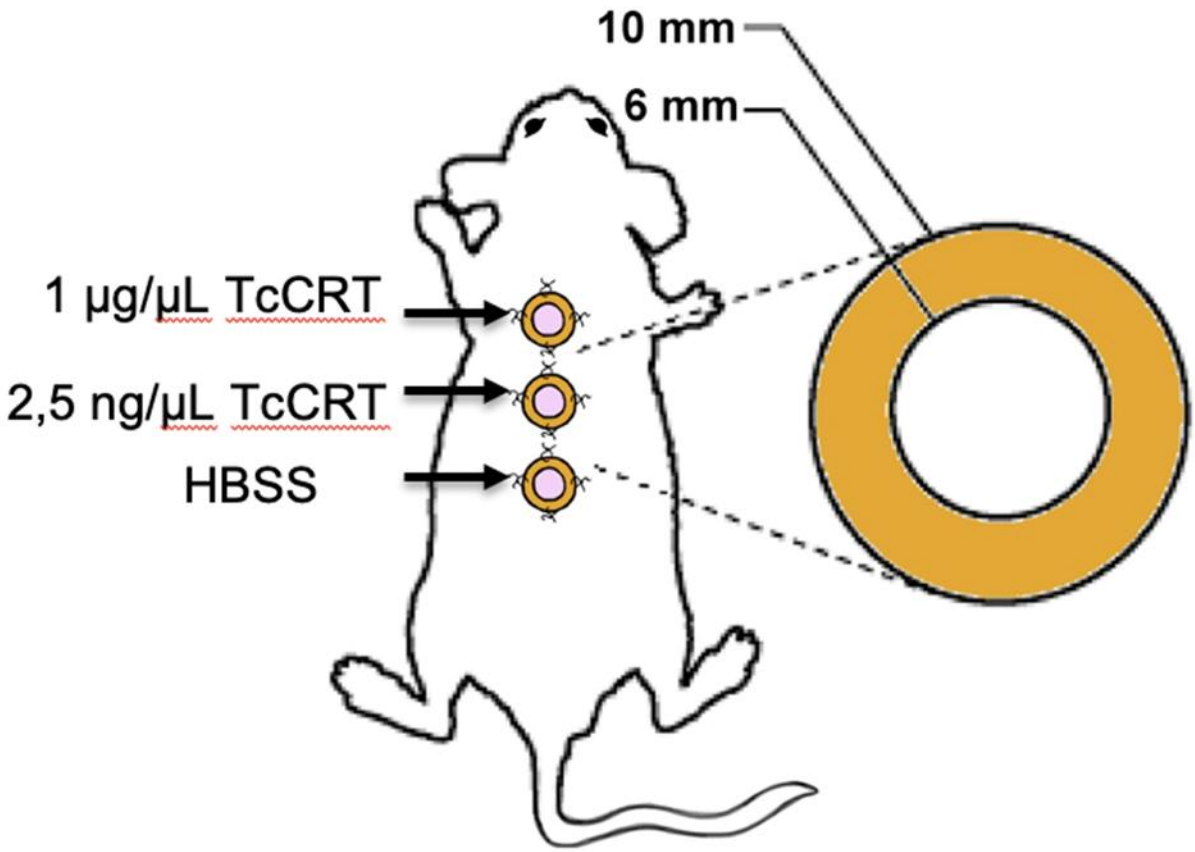

Figure 1: Distribution of experimental wounds in rats *in-vivo*. Three full-thickness skin wounds of 6mm diameter were made in the dorsal retroscapular area in each rat. 10μL of TcCRT was applied at a high concentration (1 μg/μL) in the first wound and at a low concentration (2.5 ng /μL) in the second wound and only HBSS was applied to the third wound.

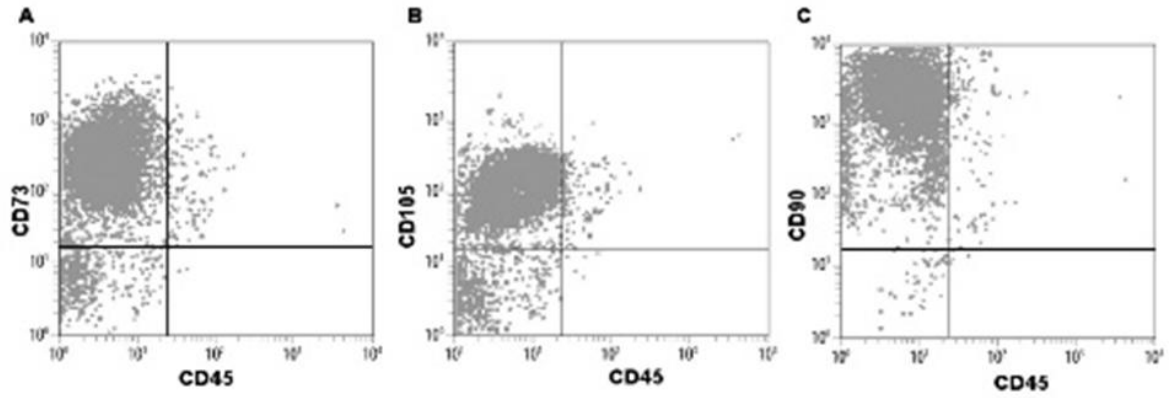

Figure 2: Flow cytometry analysis of rat ADSCs. Rat ADSCs were harvested at passage three to four and analyzed for specific cell surface antigens. Flow cytometry shows positive reaction for mesenchymal stem cell surface-associated antigens CD73 (A), CD105 (B) and CD90 (C) in contrast to minimal reaction for the CD45 negative control marker.

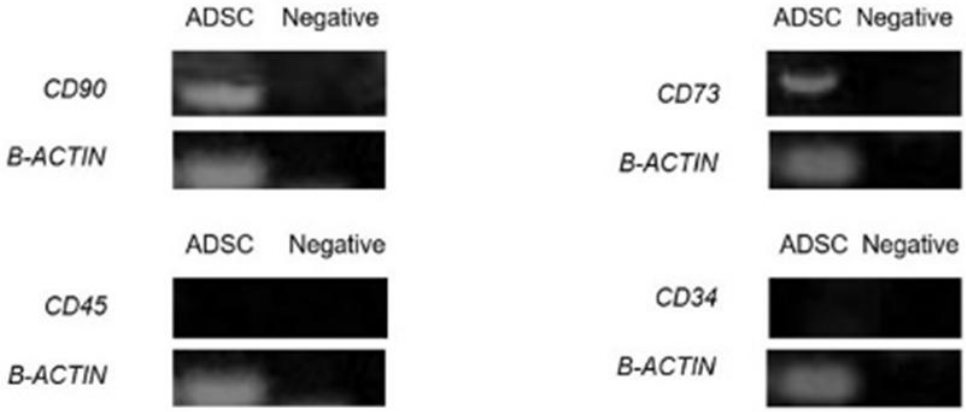

Figure 3: RT-PCR expressionof transcription factors in rat ADSCs at passage three to four. Transcription of MSC genes CD90 an CD73 was positive, but negative for Cd45 and Cd34.

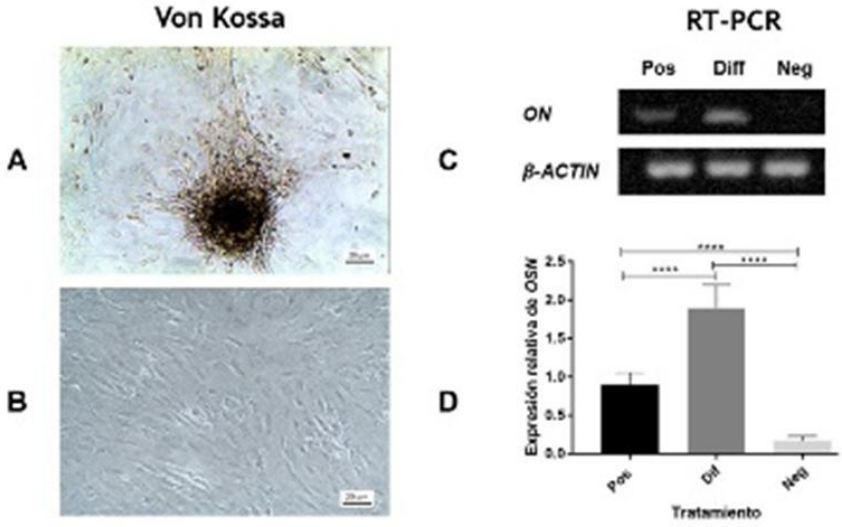

Figure 4: ADSCs after four weeks of osteogenic induction. (A) Positive von Kossa staining was observed in the osteogenic-induced cells, but (B) negative in the control. (C and D) RT-PCR shows ON mRNA expression in osteogenic-induced cells after four weeks. No expression was found in non-induced cells. Data were expressed as means ± standard deviation. **** p< 0.0001.

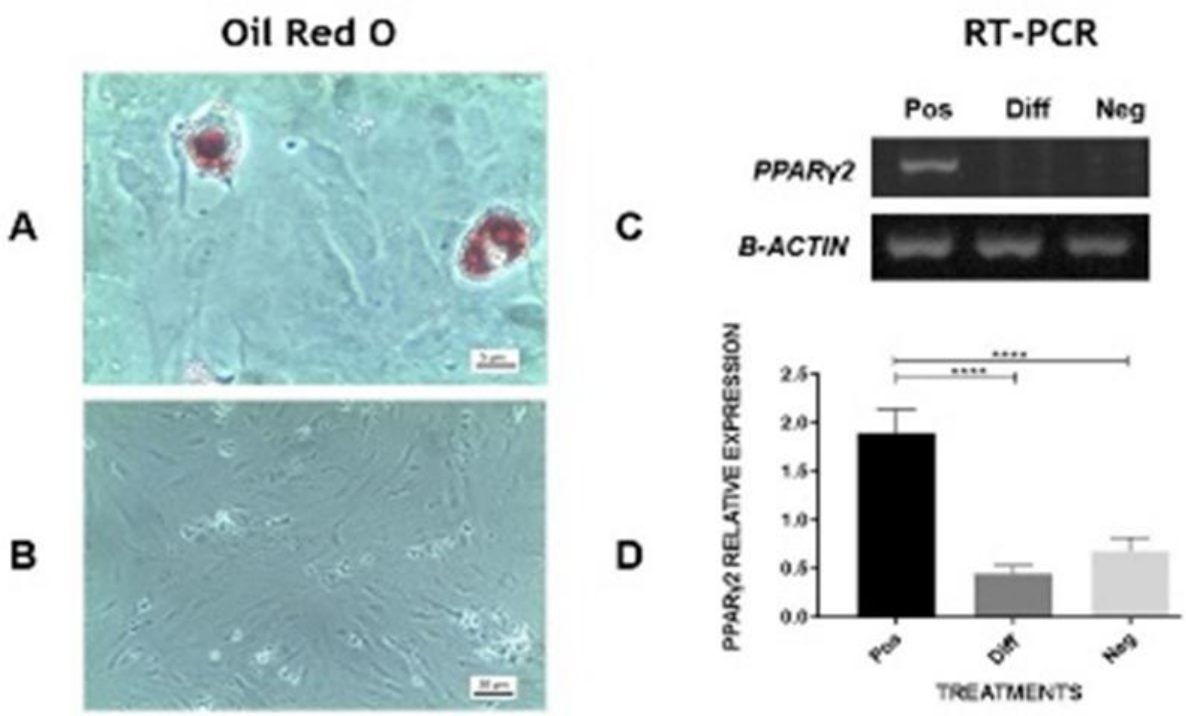

Figure 5: ADSCs after four weeks of adipogenic induction. (A) Oil Red O staining was positive in the adipogenic-induced cells and (B) negative in the control. (C and D) RT-PCR shows PPAR-γ2 mRNA expression in adipogenic-induced cells after four weeks. No detectable expression was found in adipogenic-induced cells or in non-induced cells. Data were expressed as means ± standard deviation. **** p< 0.0001.

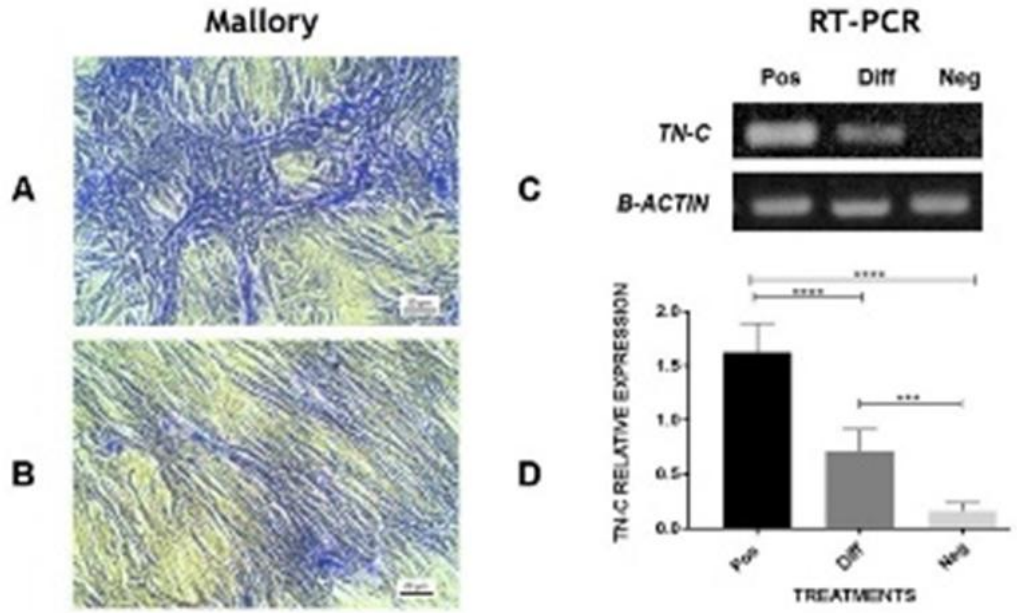

Figure 6: ADSCs after four weeks of fibroblastic induction. (A) Mallory staining was positive in the CTGF-induced cells and (B) almost negative in the control. (C and D) RT-PCR shows TN-C mRNA expression in fibroblastic-induced cells after four weeks. No detectable expression was found in adipogenic-induced cells or in non-induced cells. Data were expressed as means ± standard deviation. **** p< 0.0001 or *** p< 0.0005.

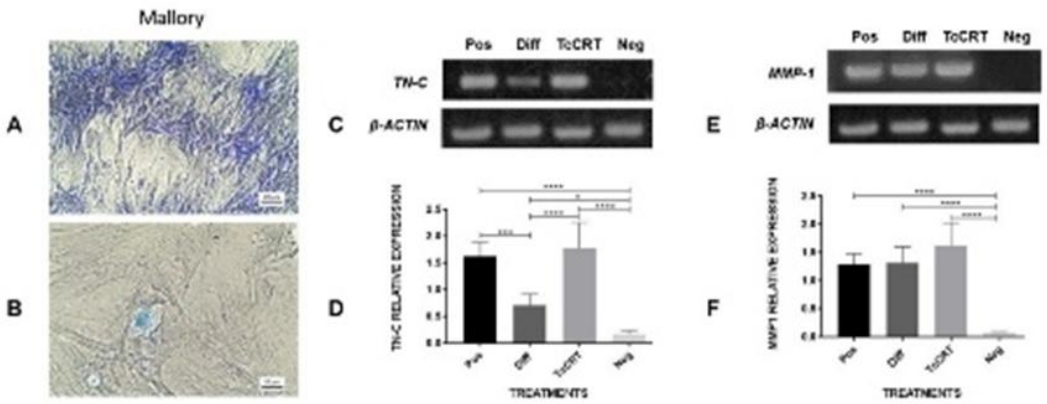

Figure 7: ADSCs after four weeks of rTcCRT-conditioned medium induction. (A) Mallory staining was positive for the rTcCRT-treated cells and (B) negative for the control. (C and D) RT-PCR shows high TN-C mRNA expression by rTcCRT-induced cells after four weeks. No detectable expression was found for non-induced cells. (E and F) RTPCR shows highmmP-1 mRNA expression for rTcCRT-induced cells after four weeks. No detectable expression was found for non-induced cells. Data were expressed as means ± standard deviation. **** p< 0.0001 or *** p< 0.0005 or * p< 0.05.

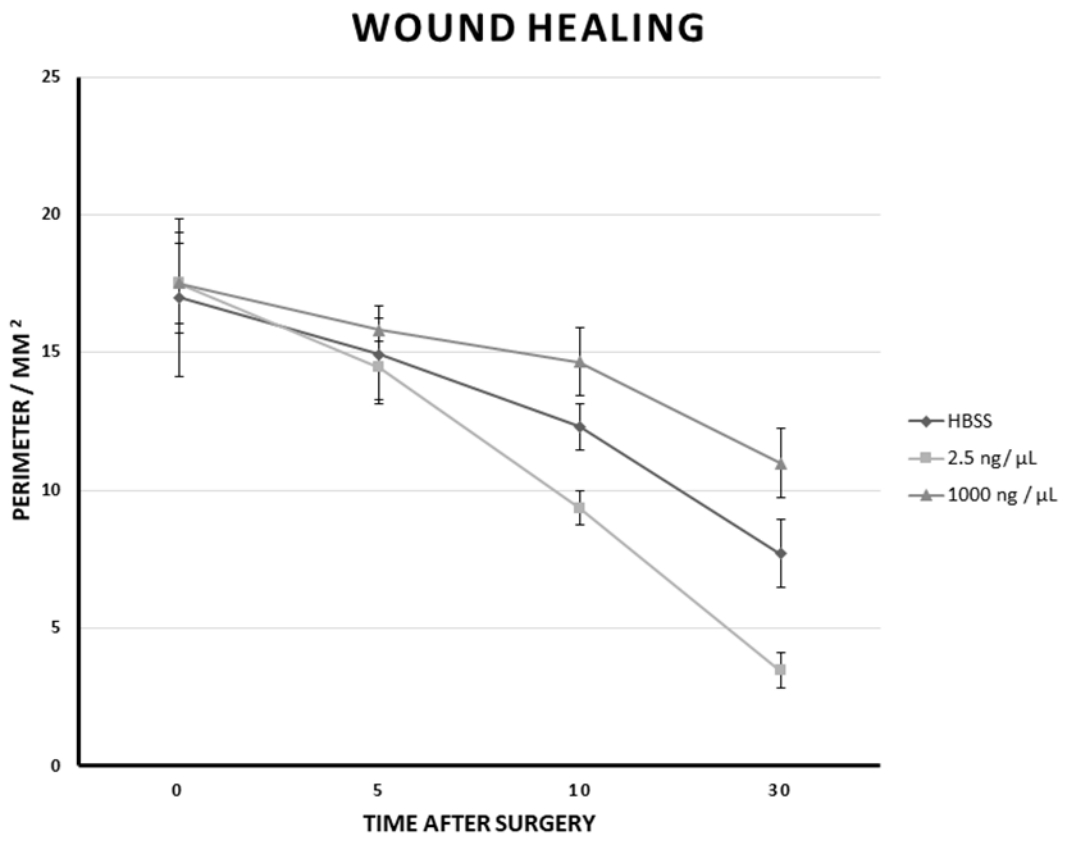

Figure 8: Wound perimeter chang es as a function of days after surgery in response to different treatments with TcCRT (low: 2.5*ng* /µL; high: 1,000ng /µL; and negative control: HBSS).

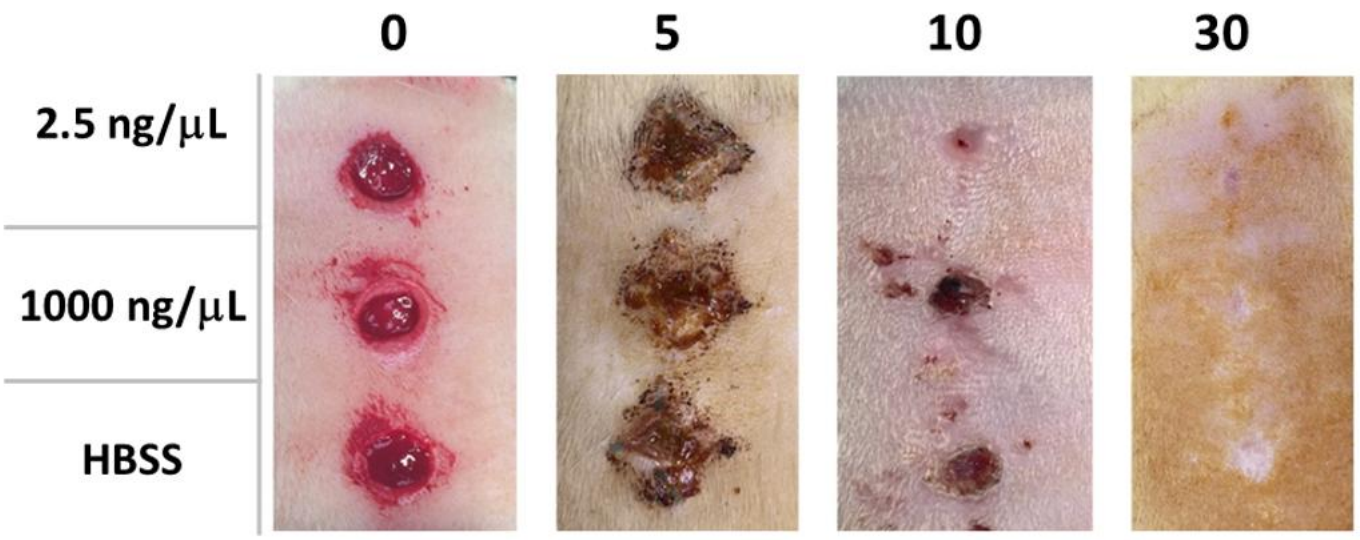

Figure 9: Photographic images of dorsal skin wounds of diabetic rats showing changes as a function of days after surgery in response to different treatments with TcCRT.

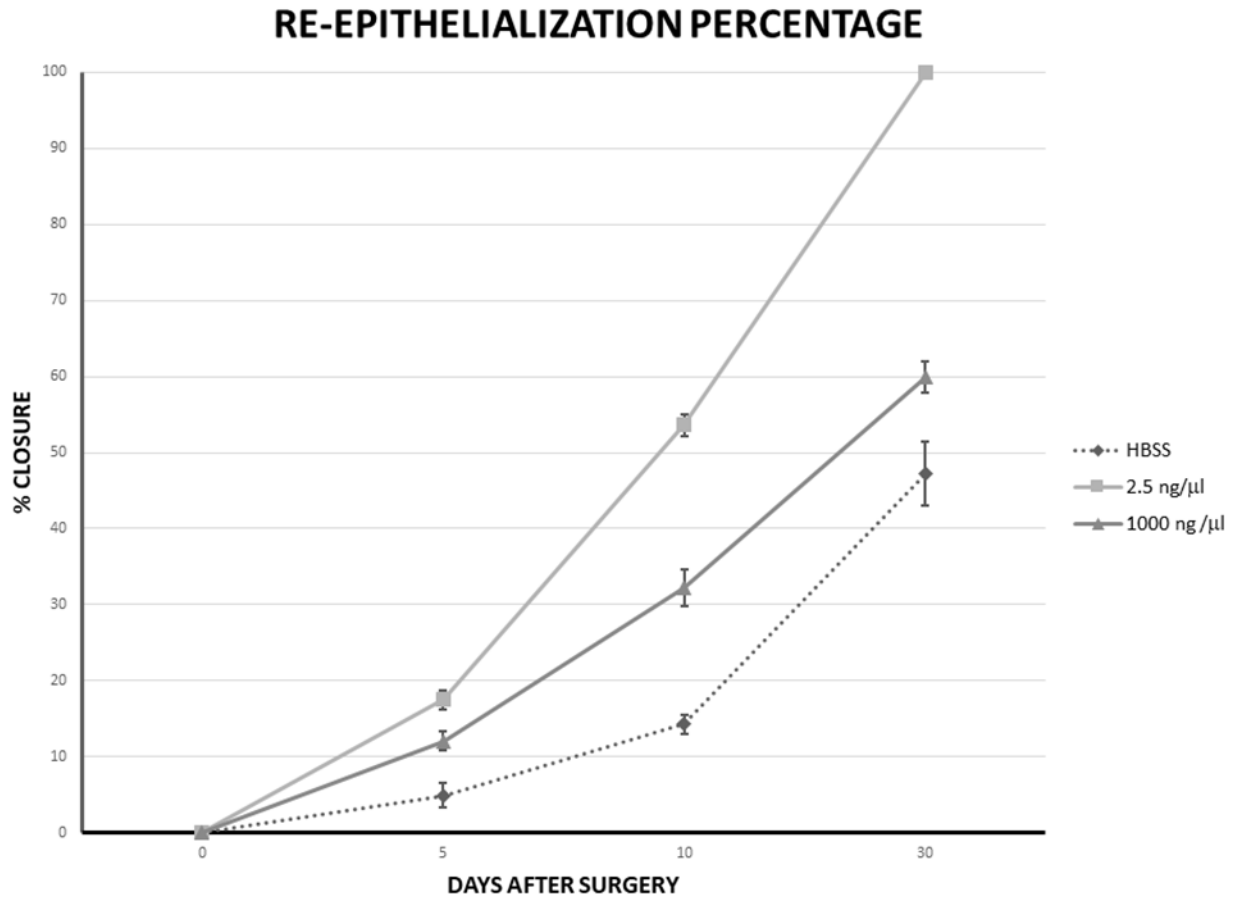

Figure 10: Re-epithelialization changes as a function of days after surgery in response to different treatments with TcCRT (low: 2.5ng /µL; high: 1,000ng /µL; and negative control: HBSS).

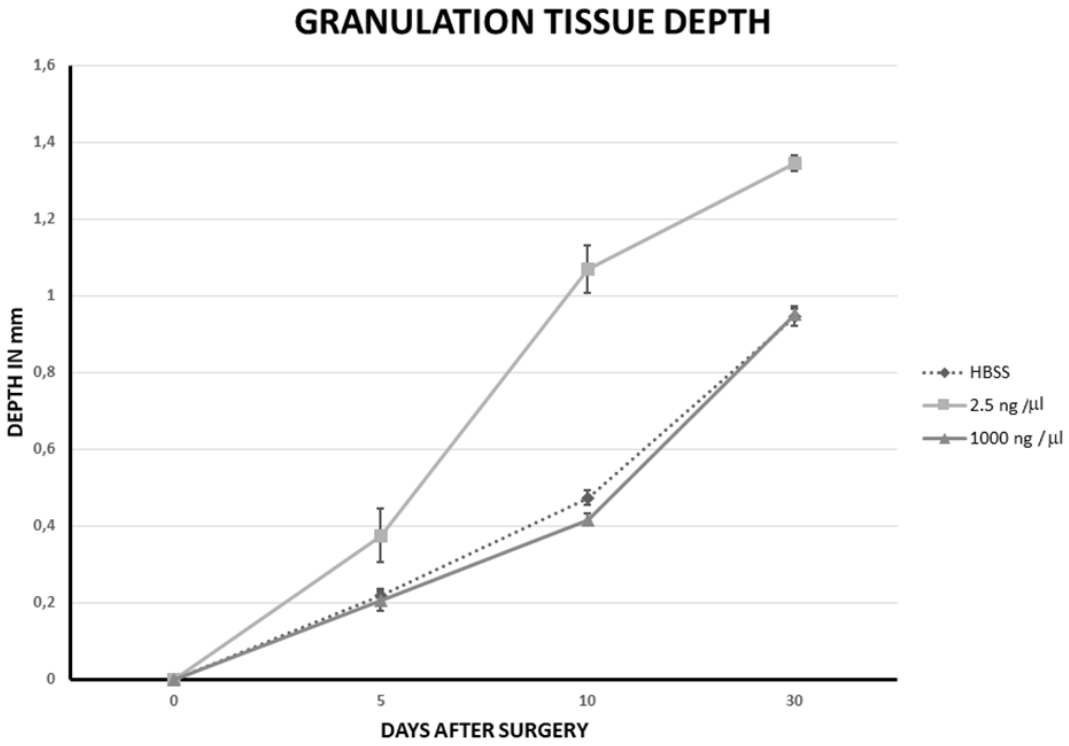

Figure 11: Granulation tissue depth in mm as a function of days after surgery in response to different treatments with TcCRT (low: 2.5ng /µL; high: 1,000ng /µL; and negative control: HBSS).

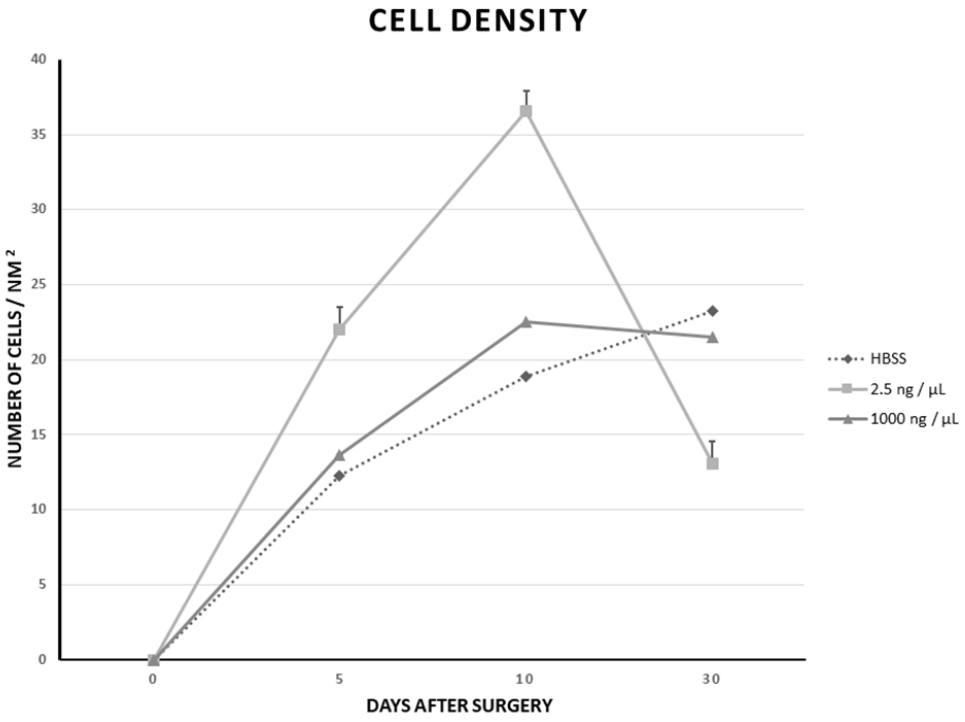

Figure 12: Cell density changes as a function of days after surgery in response to different treatments with TcCRT (low: 2.5 ng/µL; high: 1,000 ng/µL; and negative control (HBSS).

Discussion

ER stress is an important factor in fibrotic disease and it can be induced by glucose, glucosamine and oxidative stress, factors that are known to induce fibroproliferative remodeling in multiple tissues [21-24]. CRT is a 46-kDa ER protein that regulates cellular reactions to stress through its roles in the unfolded protein response and chaperone activity [25]. CRT is overexpressed in stressed ER and is dynamically expressed after skin injury and throughout wound repair with fibroblastic-type cells showing intense cytoplasmic immunoreactivity to CRT antibodies [7-11,26]. CRT extracellular functions have been tested in various *in-vitro* and *in-vivo* assays, demonstrating a great influence on skin repair and other processes, such as migration and proliferation of epithelial and mesenchymal cells, ang iogenesis inhibition, antitumor effects and promotion of cell adhesion [3,5]. Platelets secrete several mediators of wound healing, such as platelet-derived growth factor, that attract and activate fibroblasts [27]. This fibroblast population of the wound can also be the result of the recruitment of multipotent Mesenchymal Stem Cells (MSCs) residing in the dermis with potential to differentiate into dermal fibroblasts [28,29].

CRT is involved in stimulating the Wnt/β-catenin signaling pathway. Overexpression of CRT correlates with increased cell adhesiveness, increased expression of N-cadherin and vinculin and decreased protein phosphorylation on tyrosine, all of which are related to the Wnt/β-catenin signaling pathway [30,31]. This signaling pathway also is involved in the orchestration of many regulatory processes in developing skin, including the early fate decisions of embryonic somatic cell migration and differentiation in primitive skin along with the morphogenesis and growth of hair follicles and other skin appendages [32]. It has also been established that Wnt-1 inhibits alkaline phosphatase activity of dental-pulp stem cells and odontoblastic differentiation [33]. The Wnt/β-catenin signaling pathway has also been associated with ADSC adipose differentiation inhibition when activated by repressing the expression of PPARγ mRNA [34-36]. CRT is also required for TGF-β stimulation of extracellular matrix under conditions of ER stress [25]. Moreover, TGF-β promotes the differentiation of stem cells into smooth muscle cells, immature cardiomyocytes, hepatic stellate cells and dendritic cells. However, TGF-β inhibits the differentiation of stem cells into adipocytes, endothelial cells and natural killer cells. Additionally, TGF-β can provide competence for early stages of osteoblastic differentiation, but at late stages, it acts as an inhibitor [37].

Our results show that diabetic ADSCs cultured for 4 weeks in added TcCRT medium display fibroblastic behavior with abundant deposits of collagen bundles and high TN-C andmmP-1 expression. TN-C andmmP-1 have been used previously as hallmarks of fibroblastic activity [38,39]. When human bone marrow MSCs were cultured in 10 to 100 ng/mL CTGF-conditioned medium, these hallmarks were overexpressed, which correlates with what was observed when CTGF was used as a positive control in our experiments [38]. These observations led us to conclude that TcCRT could be involved in the direct stimulation of ADSCs to produce fibroblast-like matrix.

One of the factors that compromises the correct repair of skin is chronic wounds. For the most part, chronic wounds originate from minor traumatic injuries, which result in healing failure in patients with underlying pathologies such as diabetic patients. Currently, chronic wounds constitute a public health problem, since they are more frequent and are associated with high treatment costs [40]. Consequently, this has led to the study of new therapeutic agents to improve cutaneous wound healing. Among these agents, we can highlight CRT protein derived from humans, rabbits or more primitive organisms such as the flagellated protozoan, Trypanozoma cruzi [2,12,13]. CRT has been investigated with *in-vitro* and *in-vivo* models and these studies show that CRT stimulates cell proliferation and migration of keratinocytes and fibroblasts in normal skin injuries. In chronic wounds of diabetic patients, these functions are affected, often resulting in healing failure [2,12,13]. However, the effect of TcCRT on chronic wounds was unknown.

The results of our study show that topical application of TcCRT on chronic wounds accelerates the re-epithelialization process. Re-epithelialization is the process of generating a new epidermis after an injury, which restores its function as a barrier. This is carried out by migration and proliferation of keratinocytes from the existing tissue that surrounds the edges of the wound [13]. Chronic wounds in diabetic patients are known to represent a failure to achieve complete re-epithelialization in the proper temporal sequence of tissue repair [41]. For this reason, a higher rate of wound re-epithelialization is one of the best indicators of better healing in a chronic wound [12]. In our study, the effect of TcCRT on skin repair could be observed from five days after the injury with treatment at the low concentration of TcCRT (2.5ng /μL). This was evident from the increased percentage of re-epithelialization compared to treatment with a 400-fold higher concentration of TcCRT (1.0μg/μL). In untreated wounds, an even lower percentage of re-epithelialization was observed. At 30 days, only wounds treated with the low concentration of TcCRT

achieved complete wound closure (100% re-epithelialization). In contrast, to achieve the same effect on the re-epithelialization process by topical application of HuCRT in diabetic rats, 5μg/μL HuCRT was needed, a dose 2,000 times higher than the low dose of TcCRT used in our study [13]. Therefore, it is shown that TcCRT is more effective than HuCRT for improving the re-epithelialization process of wounds in diabetic rats. This agrees with results obtained in normal, non-diabetic rats, where it was reported that the application of a low concentration of TcCRT of 2.5 ng/μL stimulated a greater re-epithelialization of wounds, while the same concentration of HuCRT did not [2].

On the other hand, it should be noted that although topical application of TcCRT accelerates the re-epithelialization process in cutaneous wounds of diabetic rats, it does not result in complete wound healing at ten days, which occurs with normal rat wounds under the influence of TcCRT [2]. In contrast, in our study 100% wound re-epithelialization was achieved at 30 days in diabetic rats only with the low concentration of TcCRT (2.5ng /μL). Therefore, it can be concluded that topical application of the low concentration of TcCRT accelerates the re-epithelialization process, but it fails to generate a new epidermis in the time that corresponds to the skin of a normal rat.

One of the factors that these treatments seek to improve in patients with diabetic wounds is the formation of granulation tissue, because chronic wounds in these patients are characterized by hypocellularity and low tissue formation. All of these occur as a consequence of deficient migration and proliferation of cells, which prevents correct wound closure [13]. In our study, topical application of TcCRT to the wounds of diabetic rats produced an increase in granulation tissue formation, achieving better results with the application of the low concentration of TcCRT (2.5*ng* /μL). Topical application of the high concentration of TcCRT (1μg/μL) compared to the negative controls (receiving no TcCRT treatment) were not significantly different at five to 30 days and both showed less granulation tissue formation compared to treatment with the low concentration of TcCRT. At five days of healing, wounds treated with the low concentration of TcCRT reached a neodermal thickness twice that of wounds treated with the high concentration of TcCRT and untreated wounds. At 30 days, these wounds were the only ones that came close to reaching the dermal thickness of normal rat skin (96%). In contrast, topical application of HuCRT to wounds in-vivo in diabetic rats produced a dose-dependent increase in granulation tissue formation compared to control wounds, with a greater effect achieved with a high concentration of HuCRT (5μg/μL) [13].

The reason for the differences observed in the effects of topical application of HuCRT or TcCRT could be explained by some non-homologous domain between both molecules and some conformational differences, for which it would be essential to study the structural differences between these proteins.

During the healing process, there is an initial increase in the cellularity of the neodermis forming granulation tissue, mainly due to the migration and proliferation of fibroblasts that synthesize extracellular matrix and the formation of new capillaries [13]. After this initial step, during the maturation phase, this tissue is gradually replaced by dense connective tissue and cell apoptosis occurs, ultimately leading to a relatively acellular dermis with physical properties that are comparable to normal skin [40]. Thus, lower cellularity is indicative of higher maturity. In our study, it was observed that after five and ten days of healing, the wounds treated with the low concentration of TcCRT showed a significantly higher cellularity than the wounds treated with the high concentration of TcCRT and the control wounds, which results from greater formation of granulation tissue at the low concentration of TcCRT compared to the other treatments. However, on day 30 of healing, the wounds treated with the low concentration of TcCRT presented a significantly lower cellularity, which is the result of the maturation process of the dermis and cell apoptosis. At 30 days of healing, wounds treated with the low concentration of TcCRT showed a lower cell density that is comparable to normal rat dermis. On the other hand, control wounds and those treated with the high concentration of TcCRT had double the cellular concentration compared to normal rat dermis. Therefore, after 30 days of healing, treatment with the low concentration of TcCRT (2.5ng /μL) is the most effective, achieving a greater maturity (lower cell density) of the dermis compared to less maturity with treatment at the high concentration. These results could be explained by the fact that CRT has the important function of being the obligatory mediator for the elimination of apoptotic cells by phagocytes [12]. Consequently, the exogenous application of TcCRT could facilitate the removal of these apoptotic cells, thus giving rise to a more mature dermis with less cellularity.

In addition, macroscopic observations following topical application of the low concentration of TcCRT on the wounds of diabetic rats indicated a significant decrease in the size of the wounds and a scar of better visual quality, while the wounds treated with the high concentration of TcCRT at 30 days maintained a visually unrecovered area even greater than the untreated wounds.

HuCRT and TcCRT N-terminal fragment have vasostatin-like anti-ang iogenic properties *in-vitro* and *in-vivo* when used at higher concentrations [42-44]. This conserved protein domain could explain the detrimental effects found when higher doses of TcCRT are used for wound healing in normal and diabetic rats as shown here and elsewhere [2,3]. In fact, it has been shown that CRT undergoes N-terminal cleavage to generate a fragment, vasostatin, that acts as an inhibitor of ang iogenesis by preventing endothelial cell adhesion [3,45].

Conclusion

In summary, the results of this work suggest that the application of a low concentration of TcCRT is effective in improving wound healing in experimental diabetic rats. This is due to the stimulation of adipose MSCs to produce fibroblast-like matrix as shown *in-vitro* and an improvement in the speed of re-epithelialization, the formation of granulation tissue and the maturation of the dermis in cutaneous skin wounds in diabetic rats. Further studies could provide additional evidence that TcCRT is a promising therapeutic tool for the treatment of chronic wounds.

Conflicts of Interest

The authors declare no conflict of interest in this paper.

Funding

The authors received no financial support for this research.

Acknowledgements

May this serve as a tribute to the memory of the father of mesenchymal stem cells, Professor Arnold I. Caplan (1942-2024). We are also indebted to A. Ferreira for generously providing recombinant TcCRT. This work was partially funded by grant FONDECYT 11130257 of CONICYT Chile and Regenerative Medicine Lab (BiMre).

References

1. Greives MR, Samra F, Pavlides SC, Blechman KM, Naylor SM, Woodrell CD, et al. Exogenous calreticulin improves diabetic wound healing . Wound Repair Regen. 2012;20(5):715-30.
2. Arias JI, Sepúlveda C, Bravo P, Hamilton-West C, Maldonado I, Ferreira A. Comparative effect of human and *Trypanosoma cruzi* calreticulin in wound healing . J Tissue Eng Regen Med. 2015;9(1):41-54.
3. Arias JI, Parra N, Beato C, Torres CG, Hamilton-West C, Rosas C, et al. Different *Trypanosoma cruzi* calreticulin domains mediate migration and proliferation of fibroblasts *in-vitro* and skin wound healing *in-vivo*. Arch Dermatol Res. 2018;310(8):639-50.
4. Jeffery E, Peters LR, Raghavan M. The polypeptide binding conformation of calreticulin facilitates its cell-surface expression under conditions of endoplasmic reticulum stress. J Biol Chem. 2011;286(4):2402-15.
5. Gold LI, Eggleton P, Sweetwyne MT, Van Duyn LB, Greives MR, Naylor SM, et al. Calreticulin: non-endoplasmic reticulum functions in physiology and disease. FASEB J. 2010;24(3):665-83.
6. Sawaya AP, Vecin NM, Burgess JL, Ojeh N, DiBartolomeo G, Stone RC, et al. Calreticulin: A multifunctional protein with potential therapeutic applications for chronic wounds. Front Med (Lausanne). 2023;10:1207538.
7. Kypreou KP, Kavvadas P, Karamessinis P, Peroulis M, Alberti A, Sideras P, et al. Altered expression of calreticulin during the development of fibrosis. Proteomics. 2008;8(12):2407-19.
8. Khan MI, Pichna BA, Shi Y, Bowes AJ, Werstuck GH. Evidence supporting a role for endoplasmic reticulum stress in the development of atherosclerosis in a hyperglycaemic mouse model. Antioxid Redox Signal. 2009;11(9):2289-98.
9. Pan C, Giraldo GS, Prentice H, Wu JY. Taurine protection of PC12 cells against endoplasmic reticulum stress induced by oxidative stress. J Biomed Sci. 2010;17 Suppl 1:S17.
10. Jia L, Xu M, Zhen W, Shen X, Zhu Y, Wang W, et al. Novel anti-oxidative role of calreticulin in protecting A549 human type II alveolar epithelial cells against hypoxic injury. Am J Physiol Cell Physiol. 2008;294(1):C47-55.

11. Kelsen SG, Duan X, Ji R, Perez O, Liu C, Merali S. Cigarette smoke induces an unfolded protein response in the human lung: A proteomic approach. Am J Respir Cell Mol Biol. 2008;38(5):541-50.
12. Nanney LB, Woodrell CD, Greives MR, Cardwell NL, Pollins AC, Bancroft TA, et al. Calreticulin enhances porcine wound repair by diverse biological effects. Am J Pathol. 2008;173(3):610-30.
13. Greives MR, Samra F, Pavlides SC, Blechman KM, Naylor SM, Woodrell CD, et al. Exogenous calreticulin improves diabetic wound healing . Wound Repair Regen. 2012;20(5):715-30.
14. Aguillón JC, Ferreira L, Perez C, Colombo A, Molina MC, Wallace A, et al. Tc45, a dimorphic *Trypanosoma cruzi* immunogen with variable chromosomal localization, is calreticulin. Am J Trop Med Hyg. 2000;63:306-12.
15. Ferreira V, Molina MC, Valck C, Rojas A, Aguilar L, Ramírez G, et al. Role of calreticulin from parasites in its interaction with vertebrate hosts. Mol Immunol. 2004;40(17):1279-91.
16. Toledo V, Ramirez G, Valck C, Lopez N, Ribeiro CH, Maldonado I, et al. Comparative *in-vivo* antiang iogenic effects of calreticulin from *Trypanosoma cruzi* and Homo sapiens sapiens. Biol Res. 2010;43(3):287-9.
17. Vélez S, Gómez L, Tapia D, Guerrero E, Morán J. Standardization of the diabetes type 1 experimental model induced by streptozotocin in Sprague-Dawley rats. Rev Med Cient. 2015;28(1):4-13.
18. Vieira NM, Brandalise V, Zucconi E, Secco M, Strauss BE, Zatz M. Isolation, characterization and differentiation potential of canine adipose-derived stem cells. Cell Transplant. 2010;19(3):279-89.
19. Yuda A, Maeda H, Fujii S, Monnouchi S, Yamamoto N, Wada N, et al. Effect of CTGF/CCN2 on osteo/cementoblastic and fibroblastic differentiation of a human periodontal ligament stem/progenitor cell line. J Cell Physiol. 2015;230:150-9.
20. Michaels J, Churgin SS, Blechman KM, Greives MR, Aarabi S, Galiano RD, et al. db/db mice exhibit severe wound-healing impairments compared with other murine diabetic strains in a silicone-splinted excisional wound model. Wound Repair Regen. 2007;15(5):665-70.
21. Lenna S, Trojanowska M. The role of endoplasmic reticulum stress and the unfolded protein response in fibrosis. Curr Opin Rheumatol. 2012;24.
22. Takahashi N, Harada M, Hirota Y, Nose E, Azhary JMK, Koike H, et al. Activation of endoplasmic reticulum stress in granulosa cells from patients with polycystic ovary syndrome contributes to ovarian fibrosis. Sci Rep. 2017;7:10824.
23. Kabala PA, Ang iolilli C, Yeremenko N, Grabiec AM, Giovannone B, Pots D, et al. Endoplasmic reticulum stress cooperates with Toll-like receptor ligation in driving activation of rheumatoid arthritis fibroblast-like synoviocytes. Arthritis Res Ther. 2017;19:207.
24. Zhang JS, Hou YL, Lu WW, Ni XQ, Lin F, Yu YR, et al. Intermedin(1-53) protects against myocardial fibrosis by inhibiting endoplasmic reticulum stress and inflammation induced by homocysteine in apolipoprotein E-deficient mice. J Atheroscler Thromb. 2016;23:1294-306.
25. Zimmerman KA, Graham LV, Pallero MA, Murphy-Ullrich JE. Calreticulin regulates transforming growth factor-β-stimulated extracellular matrix production. J Biol Chem. 2013;288:14584-98.
26. Gold LI, Rahman M, Blechman KM, Greives MR, Churgin S, Michaels J, et al. Overview of the role for calreticulin in the enhancement of wound healing through multiple biological effects. J Invest Dermatol Symp Proc. 2006;11:57-65.
27. Sing er AJ, Clark RAF. Cutaneous wound healing . N Eng l J Med. 1999;341:738-46.
28. Fernandes KJ, McKenzie IA, Mill P, Smith KM, Akhavan M, Barnabé-Heider F, et al. A dermal niche for multipotent adult skin-derived precursor cells. Nat Cell Biol. 2004;6:1082-93.
29. Toma JG, Akhavan M, Fernandes KJ, Barnabé-Heider F, Sadikot A, Kaplan DR, et al. Isolation of multipotent adult stem cells from the dermis of mammalian skin. Nat Cell Biol. 2001;3:778-84.
30. Fadel MP, Szewczenko-Pawlikowski M, Leclerc P, Dziak E, Symonds JM, Blaschuk O, et al. Calreticulin affects beta-catenin-associated pathways. J Biol Chem. 2001;276:27083-9.
31. Groenendyk J, Michalak M. Disrupted WNT signaling in mouse embryonic stem cells in the absence of calreticulin. Stem Cell Rev Rep. 2014;10:191-206.
32. Lim X, Nusse R. Wnt signaling in skin development, homeostasis and disease. Cold Spring Harb Perspect Biol. 2013;5:1-25.
33. Scheller EL, Chang J, Wang CY. Wnt/β-catenin inhibits dental pulp stem cell differentiation. J Dent Res. 2008;87:126-30.
34. Zhou Y, Song T, Peng J, Zhou Z, Wei H, Zhou R. SIRT1 suppresses adipogenesis by activating WNT/beta-catenin signaling *in-vivo* and *in-vitro*. Oncotarget. 2016;7:77707-20.
35. Yuan Z, Li Q, Lou S, Liu Z, Luo D, Zhang B, et al. PPARgamma and Wnt signaling in adipogenic and osteogenic differentiation of mesenchymal stem cells. Curr Stem Cell Res Ther. 2016;11:216-25.

36. Xu C, Wang J, Zhu T, Shen Y, Tang X, Fang L, et al. Cross-talking between PPAR and WNT signaling and its regulation in mesenchymal stem cell differentiation. Curr Stem Cell Res Ther. 2016;11:247-54.
37. Wang MK, Sun HQ, Xiang YC, Jiang F, Su YP, Zou ZM. Different roles of TGF-β in the multi-lineage differentiation of stem cells. World J Stem Cells. 2012;4:28-34.
38. Lee CH, Shah B, Moioli EK, Mao JJ. CTGF directs fibroblast differentiation from human mesenchymal stem/stromal cells and defines connective tissue healing in a rodent injury model. J Clin Invest. 2010;120:3340-9.
39. Han X, Bolcato AL, Amar S. Identification of genes differentially expressed in culture human osteoblasts versus human fibroblasts by DNA microarray analysis. Connect Tissue Res. 2002;43:63-75.
40. Demidova-Rice TN, Hamblin MR, Herman IM. Acute and impaired wound healing: pathophysiology and current methods for drug delivery, part 2: role of growth factors in normal and pathological wound healing: therapeutic potential and methods of delivery. Adv Skin Wound Care. 2012;25(8):349-70.
41. Frykberg RG, Banks J. Challeng es in the treatment of chronic wounds. Adv Wound Care (New Rochelle). 2015;4(9):560-82.
42. Pike SE, Yao L, Jones KD, Cherney B, Appella E. Vasostatin, a calreticulin fragment, inhibits ang iogenesis and suppresses tumor growth. J Exp Med. 1998;188:2349-56.
43. Pike SE, Yao L, Setsuda J, Jones KD, Cherney B. Calreticulin and calreticulin fragments are endothelial cell inhibitors that suppress tumor growth. Blood. 1999;94:2461-8.
44. López NC, Valck C, Ramírez G, Rodríguez M, Ribeiro C, Orellana J, et al. Antiang iogenic and antitumor effects of *Trypanosoma cruzi* calreticulin. PLoS Negl Trop Dis. 2010;4(7):e730.
45. Pike SE, Yao L, Jones KD, Cherney B, Appella E, Sakaguchi K, et al. Vasostatin, a calreticulin fragment, inhibits ang iogenesis and suppresses tumor growth. J Exp Med. 1998;188:2349-56.